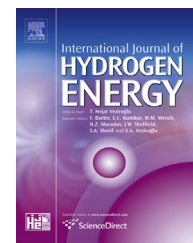


Available online at www.sciencedirect.com

ScienceDirect

journal homepage: www.elsevier.com/locate/hydro

A new approach to modelling water flooding in a polymer electrolyte fuel cell

C.Z. Qin^{*}, S.M. Hassanizadeh

Environmental Hydrogeology Group, Department of Earth Science, Faculty of Geosciences, University of Utrecht, P.O. Box 80021, 3508 TA, Utrecht, The Netherlands

ARTICLE INFO

Article history:

Received 8 July 2014

Received in revised form

12 December 2014

Accepted 9 January 2015

Available online 1 February 2015

Keywords:

Multiphase flow

Thin porous layers

Numerical modeling

Water flooding

Reduced continua model

Polymer electrolyte fuel cell (PEFC)

ABSTRACT

The distribution and migration of liquids in various layers of a PEFC is commonly modelled by the 3D flow equations. Given the fact these layers are very thin, there are major problems with such models, including heavy computational efforts and doubts in their applicability to the gas diffusion layer (GDL). Recently, a new approach for modelling multiphase flow through a stack of thin porous layers has been developed [Qin and Hassanizadeh, Int. J. Heat Mass Transfer 70 (2014) 693–708]. In this approach, which is called “*reduced continua model*”, each layer is modelled as a 2D domain with governing equations formulated in terms of thickness-averaged properties. The mass exchange between layers is prescribed by a new constitutive equation. The aim of this paper is to illustrate the implementation of the reduced continua model and show its advantages in modelling liquid water flooding in the GDL and micro porous layer (MPL) of a PEFC. We find that, in comparison to the Richards model, the reduced continua model predicts quite similar water dynamics in the MPL, but a lower steady-state water saturation in the GDL, particularly under the channel area. We provide a quantitative indication of the enormous computational efficiency of the reduced continua model as compared to the Richards model. Finally, the sensitivity studies of major material parameters of the reduced continua model have been provided.

Copyright © 2015, Hydrogen Energy Publications, LLC. Published by Elsevier Ltd. All rights reserved.

Introduction

Two-phase flow through multilayers of thin porous media is an important process in a number of industrial applications and hygiene products. One of the typical applications is the polymer electrolyte fuel cell (PEFC), which has received much attention over the past two decades [1–4]. They convert chemical energy in fuels (e.g. H₂) to electricity by means of electrochemical reactions, with the advantages of high efficiency, low/zero emission, and quick startup [5].

Usually, hundreds of PEFC units are connected in series, as a stack, to provide useful power. A schematic representation of a PEFC unit is shown in Fig. 1a. It consists of a cathode side (where air is delivered) and an anode side (where hydrogen is delivered), separated by a solid electrolyte membrane as an electrical insulator [3]. Each side consists of one bipolar plate (BP), one gas diffusion layer (GDL), one micro porous layer (MPL), and one catalyst layer (CL). Several intricate transport processes can occur in an operating PEFC, such as reactant diffusion in the gas phase, air–water flow, heat transfer, as well as electron and proton conduction [5]. An optimum water

^{*} Corresponding author. Tel.: +31 (0)30 2535084; fax: +31 (0)30 2535030.

E-mail addresses: C.Qin@uu.nl, chaozhong.qin@gmail.com (C.Z. Qin).
<http://dx.doi.org/10.1016/j.ijhydene.2015.01.035>

0360-3199/Copyright © 2015, Hydrogen Energy Publications, LLC. Published by Elsevier Ltd. All rights reserved.

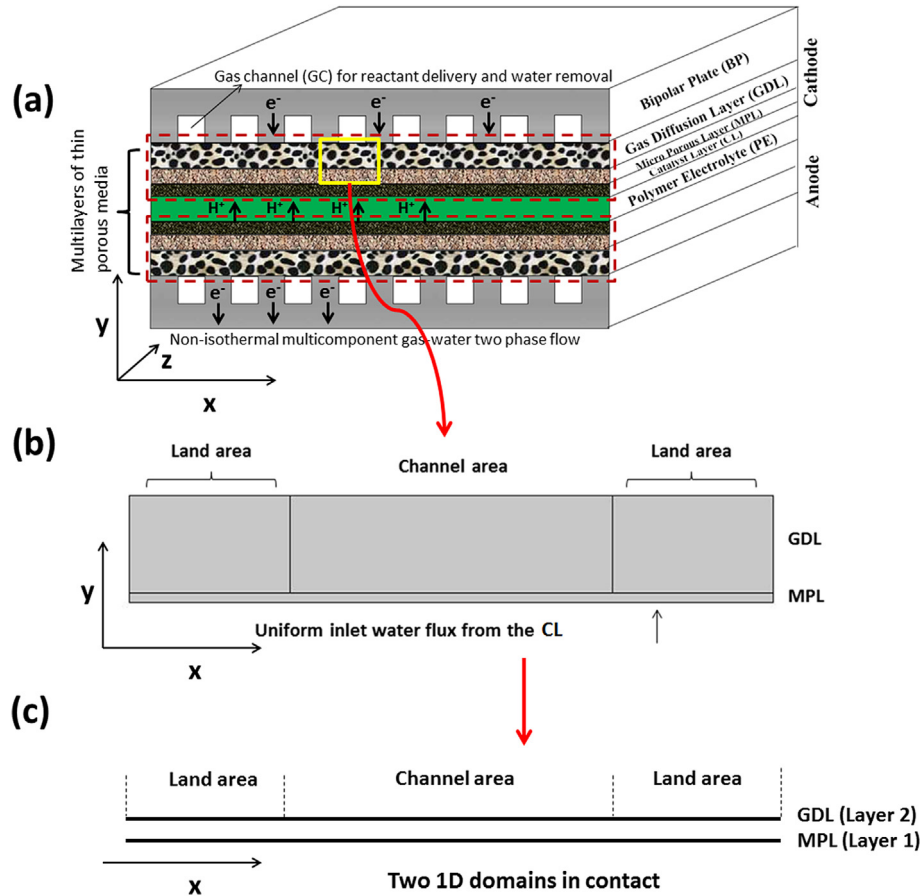


Fig. 1 – (a) Schematic representation of a PEFC unit; (b) simplified 2D computational domain used in the traditional Richards model; and (c) two 1D computational domains used in the reduced continua model.

balance is critical to the operation of PEFCs. On one hand, the solid membrane needs to attain high water content for effective ionic conduction; on the other hand, too much water accumulating in the system would result in reactant transport limitation and cell degradation [6–10]. Normally, such a situation is termed as ‘liquid water flooding’ in PEFCs.

In an operating PEFC, water is produced partly from the humidification of inlet reactants and partly from electrochemical reactions in the cathode CL. At high current densities and/or in humid environments, all diffusion layers (GDL, MPL, and CL) and GCs can become flooded, particularly on the cathode side [11]. In general, liquid water movement in a PEFC can be categorized into three subprocesses, namely: (1) liquid water production and transport in CL; (2) liquid water transport in MPL and GDL; (3) liquid water emergence at GDL-GC interface and its subsequent movement in GC. In modeling these water transport processes, a number of difficulties have been encountered with traditional Darcy-based models. First, it is a major challenge to model imperfect physical contact interfaces between neighboring porous layers with quite different material properties; e.g. between MPL and CL [12–14]. Second, there is no satisfactory approach for coupling liquid water dynamics in GC and the description of water transport in GDL [15–17]. This problem is commonly referred to as the two-phase interface treatment between free flow and

porous media flow. Last but not least, it is very questionable whether three dimensional (3D) Darcy-based models are applicable to these extremely thin porous layers. It is known that most macroscale PEFC models [2, 9, 10, and 16] are formulated in terms of averaged quantities, which are defined over an averaging domain known as the representative elementary volume (REV). A major requirement of this REV is that its size must be much larger (10–15 times) than the pore size, but much smaller than the modeling domain size [18]. This criterion cannot be satisfied in the fibrous GDL as its thickness is only 10–15 times its mean pore size. Based on the pore-scale pore-network modeling of water transport in a GDL, Rebai and Prat [19] illustrated the poor predictions of traditional Darcy-based models. In addition, 3D modeling of these interacting thin porous layers often requires heavy computational efforts, which have hindered the stack-level modeling of PEFCs.

It is interesting to point out that the conventional concept of REV does apply to the MPL, although it is even thinner than the GDL. This is because the mean pore size of MPL is several hundred nanometers [3], which is about hundred times smaller than its thickness (around 30 microns). This allows the identification of an appropriate REV. Thus, we define ‘a physically thin porous layer’ as a porous layer for which the REV length scale requirements are not satisfied along the layer

thickness. In general, this means that the layer thickness is only around one order of magnitude larger than its mean pore size. We also define ‘a geometrically thin porous layer’ for which the REV length scale requirements are satisfied but the layer thickness is much smaller than its in-plane dimensions (e.g. MPL and CL). Obviously, it could happen that a porous layer is considered to be both physically and geometrically thin.

Over the past few years, much effort has been invested into measuring GDL material properties, such as saturation-dependent effective diffusivity, intrinsic and relative permeability, and effective heat conductivity [20–23]. These material properties were directly used in 3D Darcy-based PEFC models, whereas they were all measured as thickness-averaged properties. As illustrated in Fig. 2, in traditional approach, the through-plane direction of GDL is discretized into many computational grids. Then, the layer-scale material properties are assigned to each computational grid. This is not acceptable if the layer is heterogeneous.

Because of the failure of the traditional REV concept in fibrous GDL, and extremely small thickness of MPL and CL, we were motivated to model them as thin porous layers. This approach was recently developed by Qin and Hassanizadeh [24], to which they refer as the reduced continua model. In the new approach, thin porous layers were treated as a set of 2D interacting continua stacked in series (e.g. Fig. 1c). Then, macroscale balance laws were formulated in terms of thickness-averaged material properties. The interaction between neighboring layers was accounted for by exchange terms for mass, momentum, and heat. Based on the exploitation of the second law of thermodynamics and linearization theory, the closed form of governing equations for

nonsiothermal multiphase flow through thin porous layers were provided. Here, it is worth noting that the reduced continua model does take into account the through-plane transport of thermodynamic quantities among layers. But, the detailed distribution in each layer is lumped into thickness-averaged values. In some cases, if the distribution in an individual layer is needed, a pore-scale model such as pore-network model [19] can be combined with the reduced continua model. This method is normally referred to as multi-scale modeling.

In comparison with previous 3D macroscale models, the new approach has the following distinctive advantages: (1) it is developed from rigorous thermodynamic principles; (2) it is formulated in terms of thickness-averaged material properties which are measurable; (3) it allows for modelling the effect of the contact surface between adjacent layers in a natural way; and (4) it reduces 3D modeling to 2D, leading to a very significant reduction of computational efforts. To the best of our knowledge, over the past few years, most of 3D PEFC numerical studies have been performed for a small part of PEFC unit with only one or a few GCs on each side, because of heavy computational efforts [25–27].

The main objective of this work is to apply the reduced continua model to the numerical study of liquid water flooding in the cathode GDL and MPL of a PEFC. In particular, we have parameterized the material property which determines the water exchange between layers. To illustrate the advantages of the reduced continua model and its difference with the traditional Darcy-based models, we conducted numerical studies using a traditional Darcy-based model (i.e. the Richards model which has been widely used in PEFC modeling [28,29]) as well as the reduced continua model. We focus on water dynamics in the two thin porous layers. Species transport and electrochemical reactions are not considered in this work. It is worth noting that this work is not aiming to provide guidelines for optimum water management and fuel cell operations; and it is not aiming to validate the reduced continua model against the Richards model. But, we demonstrate that the reduced continua model is able to capture key dynamic behaviors of liquid water transport through the two thin porous layers with different material properties.

The paper is organized as follows. First, the problem under study is described. Then, the employed numerical models, namely, the Richards model and the reduced continua model, are presented in detail in Section Numerical models. In Section Description of numerical simulations, we give the description of numerical simulations in this work. Numerical results are presented and discussed with an emphasis on the comparison between the two models in Section Results and discussion. Finally, we end up with main conclusions and future perspectives.

Problem description

In the operation of a PEFC, the cathode side is prone to being flooded first, because of water generation in the cathode CL and water migration from the anode under the electro-osmotic drag (EOD). Excessive liquid water in the CL migrates through the MPL and GDL into the GCs under capillary

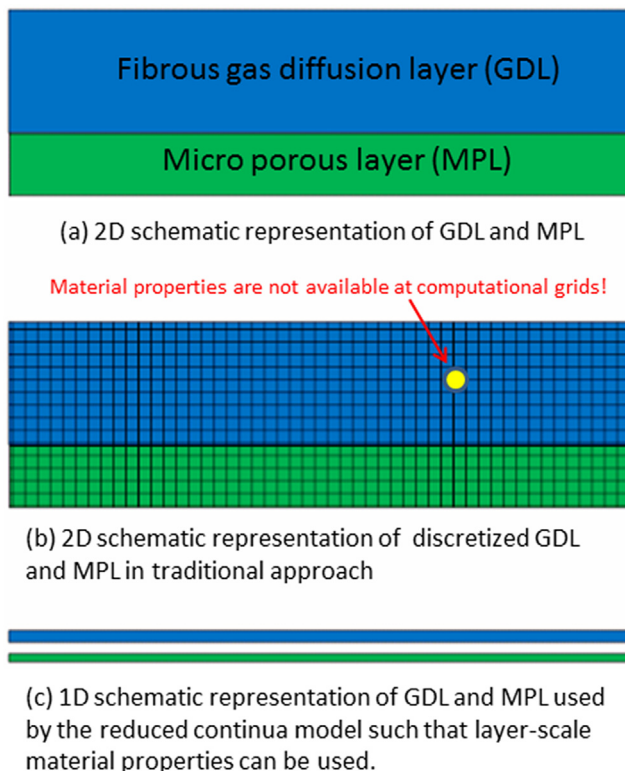


Fig. 2 – Schematic representation of GDL and MPL.

action. Finally, most of water will be removed out of the cell under gas drag force in the GCs. Fig. 1a shows a schematic representation of a PEFC unit. It can be seen that on each side many parallel channels are grooved in the BP which are used to deliver humidified reactants into the system.

Here, we concentrate on liquid water dynamics in the cathode MPL and GDL. The CL is assumed to deliver liquid water to the MPL, and a simplified boundary condition at the exit of GDL to the GC is employed. For simplicity and without loss of generality, we assume a uniform water influx. As a result, for the case of the Richards model, the 3D domain of MPL and GDL reduces to a 2D modeling domain, which is shown in Fig. 1b. Here, the cross section of the 3D domain along the GC flow direction is used with two land areas and one channel area (marked by a yellow rectangle in Fig. 1a) (in web version). For the case of the reduced continua model, the 2D computational domain will be further reduced to two interacting 1D domains which are in contact as shown in Fig. 1c. For the reduced continua model, the boundary conditions of the MPL inlet and the GDL outlet appear as source and sink terms in the governing equations, respectively. We emphasize that taking the cross sections of GDL and MPL as the computational domain is just for simplicity. Its extension to a whole PEFC unit is straightforward.

Numerical models

Richards model

Governing equations

The problem under study can be generalized as ‘isothermal immiscible air–water flow from a fine porous layer to a coarse porous layer’. The disparity in properties between air and water allows us to make some assumptions for the system of two-fluid equations. The Richards assumption states that the air has sufficiently low viscosity that we can assume it to be inviscid. In that case, it is infinitely mobile and can move without any appreciable pressure gradients. However, in the PEFC application, due to the consumption of gaseous reactants in CL, a small pressure drop builds up across diffusion layers. As a result, the Richards model would slightly underestimate the water flooding [30]. Nevertheless, for the purpose of this study, we select the Richards model for simplicity. Its extension to the two-phase Darcy’s law is straightforward. First, the mass conservation of liquid water is written as:

$$\frac{\partial}{\partial t}(\rho^w \varepsilon s^w) + \nabla \cdot (\rho^w \mathbf{v}^w) = 0 \quad (1)$$

where the superscript w denotes the liquid water, ρ^w is the mass density, ε is the porosity, s^w is the water saturation, and \mathbf{v}^w is the Darcy velocity (i.e. superficial velocity). The latter is given by the two-phase Darcy’s law:

$$\mathbf{v}^w = -\frac{k^r \mathbf{k}}{\mu^w} (\nabla p^w - \rho \mathbf{g}) \quad \text{with} \quad \mathbf{k} = \begin{bmatrix} k_i & 0 \\ 0 & k_t \end{bmatrix} \quad (2)$$

where \mathbf{k} is the intrinsic permeability tensor composed of the in-plane permeability k_i and through-plane permeability k_t , k^r is the water relative permeability, μ is the dynamic viscosity, p is the pressure, and \mathbf{g} is the gravity vector. Note that both

intrinsic permeability and relative permeability are material properties which need to be determined by experiments. In addition, the two phase pressures are linked by the macroscopic capillary pressure as:

$$p^a - p^w = p^c \quad (3)$$

where p^a is the air pressure, and p^c is the capillary pressure which is traditionally assumed to be a function of only water saturation. Because a constant air pressure is assumed, Eq. (3) can be recast as:

$$\nabla p^w = -\nabla p^c = -\frac{dp^c}{ds^w} \nabla s^w \quad (4)$$

Due to the small dimensions of computational domain, we can neglect the gravity effect. Then, substitution of Eq. (2) and Eq. (4) into Eq. (1) yields the Richards form of water transport equation:

$$\frac{\partial}{\partial t}(\rho^w \varepsilon s^w) + \nabla \cdot \left(\rho^w \frac{k^r k^0}{\mu^w} \frac{dp^c}{ds^w} \nabla s^w \right) = 0 \quad (5)$$

In the PEFC modeling, the Leveret-J function has been widely used to give the capillary pressure as a function of water saturation [9]:

$$p^c = \sigma \cos \theta \left(\frac{\varepsilon}{k_t} \right)^{1/2} J(s^w) \quad (6)$$

$$J(s^w) = \begin{cases} 1.417(1-s^w) - 2.12(1-s^w)^2 + 1.263(1-s^w)^3 & \theta \leq 90^\circ \\ 1.417s^w - 2.12(s^w)^2 + 1.263(s^w)^3 & \theta > 90^\circ \end{cases} \quad (7)$$

Here, σ is the air–water surface tension, and θ is the contact angle of porous medium. The relative permeability is also assumed to be a function of saturation: $k^r = (s^w)^3$.

Finally, to solve the water transport equation (5), additional MPL-GDL interface boundary conditions are needed. We assume the continuity of water flux and water pressure. This also ensures the continuity of capillary pressure. The resulting interface conditions are:

Pressure continuity:

$$\sigma \cos \theta \left(\frac{\varepsilon}{k_t} \right)^{1/2} J(s^w) \Big|_{\text{MPL}} = \sigma \cos \theta \left(\frac{\varepsilon}{k_t} \right)^{1/2} J(s^w) \Big|_{\text{GDL}} \quad (8)$$

Flux continuity:

$$-\rho^w k^r k_t \frac{dp^c}{\mu^w} \frac{\partial s^w}{\partial y} \Big|_{\text{MPL}} = -\rho^w k^r k_t \frac{dp^c}{\mu^w} \frac{\partial s^w}{\partial y} \Big|_{\text{GDL}} \quad (9)$$

Here, the subscript MPL denotes that the variables before the vertical bar are evaluated on the MPL side, whereas the subscript GDL denotes the variables are evaluated on the GDL side. Under the condition of pressure continuity, because of the difference in capillary pressure curves, water saturation is expected to be discontinuous at the interface.

Boundary conditions

The condition of uniform water flux is imposed at the bottom of MPL, which is given as:

$$j^w = \frac{I}{2F} \frac{M_{\text{H}_2\text{O}}}{\rho^w} \quad (10)$$

where I is the operating current density, F is the Faraday's constant, and M_{H_2O} is the molecular weight of water. Note that we assume that on the cathode side the back-diffused water through the membrane just balances the water from the EOD.

At the top of GDL, no-flux condition is imposed at the two land areas, whereas a known water saturation is assumed at the channel area. As in most previous studies, we assume the saturation to be zero. That can be justified by the fact that high gas flow rates in the GC will remove emerging liquid water droplets effectively. Otherwise, water coverage effect [31,32] will be of concern which is beyond the scope of the present study. At the side boundaries, no-flux conditions are assumed.

Reduced continua model

Governing equations

In the reduced continua model, the 2D computational domain is reduced to two 1D domains as shown in Fig. 1c. Consistent with the Richards assumption, here we only focus on liquid water transport in the two thin layers. The gas phase is assumed to be at constant pressure. First, the mass conservation equations of liquid water in the two layers are given as [24]:

$$\frac{\partial}{\partial t}(b_1 \rho^w \varepsilon_1 s_1^w) + \frac{\partial}{\partial x}(b_1 \rho^w v_1^w) = S_{w1}^T + S_{w1}^B \quad (11)$$

$$\frac{\partial}{\partial t}(b_2 \rho^w \varepsilon_2 s_2^w) + \frac{\partial}{\partial x}(b_2 \rho^w v_2^w) = S_{w2}^B + S_{w2}^T \quad (12)$$

where the subscripts 1 and 2 denote the MPL and GDL, respectively, b is the layer thickness, v is the superficial in-plane water velocity, x is the in-plane direction, S_{w1}^B is the water input through the bottom of MPL which is pre-specified, S_{w1}^T accounts for the water transport out of the GDL through its top, and the water exchange through the MPL-GDL interface is taken into account by S_{w1}^T and S_{w2}^B .

One difficulty is how to model the dynamic water exchange at the MPL-GDL interface. Our previous thermodynamic studies [24] show that the mass exchange of any phase between the two layers arises from the differences in the sum of temperature-weighted Gibbs free energies, kinetic energies, and internal energies between the two layers. If we assume slow flow in thin porous layers (this is quite true in the PEFC application where water velocity is on the order of 10^{-4} m/s), the effect of kinetic energies can be neglected. Then, Qin and Hassanizadeh [24] have shown that the layer-layer mass exchange of water can be approximated by:

$$S_{w1}^T = -S_{w2}^B = \Pi_m(p_2^w - p_1^w) \quad (13)$$

where Π_m [s/m] is a material property of the two layers, p_1^w is the average water pressure in the MPL, p_2^w is the average water pressure in the GDL. In principle, the coefficient Π_m should be determined experimentally. But, in the absence of experimental data, in this work, we propose an equation for it, based on the properties of MPL and GDL, in the following form:

$$\Pi_m = \frac{2}{b_1 + b_2} \rho^w \bar{k}_t f(s_1^w, s_2^w) \quad (14)$$

where \bar{k}_t is referred to as the effective intrinsic through-plane permeability of the two layers, and a general saturation

function $f(s_1, s_2)$ is used to represent the relative permeability for liquid water transport through the layer-layer interface, which is assumed to be a function of the two saturations. It is worth noting that our postulation of Eq. (14) is partially based on assuming the layer-scale two-phase Darcy's law in the through-plane direction. Its validation and improvement need to be done by further experimental studies.

Based on the layer-scale single-phase Darcy's law, the effective intrinsic permeability of the two layers can be given as:

$$\bar{k}_t = \frac{b_1 + b_2}{b_1 k_2^t + b_2 k_1^t} k_1^t k_2^t \quad (15)$$

The saturation function f is assumed to have the following form:

$$f(s_1^w, s_2^w) = \frac{(s_1^w)^{\gamma_1} + (s_2^w)^{\gamma_2}}{2} \quad (16)$$

where γ_1 and γ_2 are the two fitting parameters. One essential feature of $f(s_1^w, s_2^w)$ should be that it becomes unity when the two thin layers are fully saturated with liquid water.

According to the thermodynamic studies [24], the full form of fluid motion equation in each thin layer may be given as (note that the motion is in the in-plane direction, and uniform layer thickness is assumed):

$$v_1^w = -\frac{k_1^r k_1^i}{\mu^w} \left(\frac{\partial p_1^w}{\partial x} - \rho^w g_x + \frac{\Omega}{s_1^w} \frac{\partial s_1^w}{\partial x} - \frac{\rho^w}{b_1} T_1^B \right) \quad (17)$$

$$v_2^w = -\frac{k_2^r k_2^i}{\mu^w} \left(\frac{\partial p_2^w}{\partial x} - \rho^w g_x + \frac{\Omega}{s_2^w} \frac{\partial s_2^w}{\partial x} - \frac{\rho^w}{b_2} T_2^T \right) \quad (18)$$

where Ω is the wettability potential [24], T_1^B is the in-plane stress input from the bottom of MPL, and T_2^T is the in-plane stress input from the top of GDL. Both are zero in the present case studies.

If we neglect gravity effect and non-Darcian terms, we obtain the following 1D two-phase Darcy equations for water transport in the two layers:

$$v_1^w = -\frac{k_1^r k_1^i}{\mu^w} \frac{\partial p_1^w}{\partial x} \quad (19)$$

$$v_2^w = -\frac{k_2^r k_2^i}{\mu^w} \frac{\partial p_2^w}{\partial x} \quad (20)$$

In order to get a closed set of governing equations, we still need to specify equations for the water input to the bottom of MPL, S_{w1}^B , and the water flux out of the top of GDL, S_{w2}^T . The equation for S_{w1}^B is similar to the boundary condition (10) for the Richards model:

$$S_{w1}^B = \frac{I}{2F} M_{H_2O} \quad (21)$$

The water flux out of the GDL, S_{w2}^T , is assumed to be given by an equation based on the Darcy's law:

$$S_{w2}^T = -\rho^w \frac{k_2^r k_2^i}{\mu^w} \frac{p_2^w - p^0}{b_2/d} \quad (22)$$

where p^0 is the water pressure in the GC, and coefficient d is a geometric constant related to the location of average pressure

in the GDL. If the value of average pressure can be assigned to the middle of GDL, then $d=2.0$. If there is no liquid water in the GC, we set p^0 to zero. This is in correspondence with the upper boundary condition for the Richards model where we assumed saturation in the GC to be zero. Finally, under the land areas (i.e. $0 \leq x \leq 0.0005$ and $0.0015 \leq x \leq 0.002$), no water can go out of the GDL. Therefore, $S_w^T|_2$ is set to zero.

Combining equations (11)–(16) and (19)–(22) results in the following two equations, that combined with equations (6) and (7), can be solved for the average saturations s_1^w and s_2^w :

$$\begin{aligned} \frac{\partial}{\partial t} (b_1 \rho^w \varepsilon_1 s_1^w) + \frac{\partial}{\partial x} \left(b_1 \rho^w \frac{k_1^r k_1^i}{\mu^w} \frac{dp_1^c}{ds_1^w} \frac{\partial s_1^w}{\partial x} \right) \\ = - \frac{2}{b_1 + b_2} \rho^w \frac{\bar{k}_t}{\mu^w} \frac{(s_1^w)^{\gamma_1} + (s_2^w)^{\gamma_2}}{2} (p_2^c - p_1^c) + \frac{I}{2F} M_{H_2O} \end{aligned} \quad (23)$$

$$\begin{aligned} \frac{\partial}{\partial t} (b_2 \rho^w \varepsilon_2 s_2^w) + \frac{\partial}{\partial x} \left(b_2 \rho^w \frac{k_2^r k_2^i}{\mu^w} \frac{dp_2^c}{ds_2^w} \frac{\partial s_2^w}{\partial x} \right) \\ = \frac{2}{b_1 + b_2} \rho^w \frac{\bar{k}_t}{\mu^w} \frac{(s_1^w)^{\gamma_1} + (s_2^w)^{\gamma_2}}{2} (p_2^c - p_1^c) \end{aligned} \quad (24)$$

$$- \begin{cases} 0 & \text{under land} \\ \rho^w \frac{k_2^r k_2^i}{\mu^w} \frac{p_2^c - p^0}{b_2/d} & \text{under channel} \end{cases}$$

Boundary conditions

Compared to the 2D modeling with the Richards model, the boundary conditions for the reduced continua model are very simple. Only no-flux conditions are imposed at the two ends in the x direction as shown in Fig. 1c. As stated above, the boundary conditions at the bottom of MPL and the top of GDL appear as the source and sink terms in the governing equations (23) and (24), respectively.

Description of numerical simulations

Both numerical models described in the previous section were solved in COMSOL, which is a finite-element-based commercial software. Simulations were done for a base case scenario and many scenarios with variations around the base case. Values of various geometric, physical and operating parameters for the base case are listed in Table 1. In the case of the 2D Richards model, the modeling domain is shown in Fig. 1b. The width is $2000 \mu\text{m}$, and the thicknesses of GDL and MPL are $300 \mu\text{m}$ and $30 \mu\text{m}$, respectively. The modeling domain for the reduced continua model is also $2000 \mu\text{m}$ wide as shown in Fig. 1c. Both GDL and MPL are hydrophobic and have the same contact angle of 110° . Also, mesh independence studies have been conducted in both models. We used 25025 triangular elements for the Richards model, while 150 edge elements were used for the reduced continua model.

In the reduced continua model, there are two important fitting parameters: γ_1 and γ_2 , whose values need to be provided. Ideally, the two parameters should be determined experimentally; for example by performing steady-state experiments with a constant water flux through the layers and measuring the average saturation and pressure of each layer. But, in the absence of experimental data, instead of arbitrarily

Table 1 – Geometric, physical, and operating parameters.

Parameter	Value + units
GDL dimensions: $x \times y$	$2\text{e-}3 \times 3\text{e-}4 \text{ m}$
MPL dimensions: $x \times y$	$2\text{e-}3 \times 3\text{e-}5 \text{ m}$
GDL/MPL porosity	0.6/0.4
GDL intrinsic permeability, in-plane/through-plane [13].	$1.5\text{e-}13/1.5\text{e-}13 \text{ m}^2$
MPL intrinsic permeability	$3\text{e-}14 \text{ m}^2$
GDL/MPL contact angle	$110^\circ/110^\circ$
Air-water surface tension	0.0625 N/m
Operating current density	$2\text{e}4 \text{ A/m}^2$
Air gauge pressure	0 Pa
Faraday's constant	96487 C
Water density at 80°	972 kg/m^3
Dynamic viscosity of water	$3.5\text{e-}4 \text{ Pa s}$
Molecular weight of water	0.018 kg/mol
Relative location of average pressure in GDL, d	$2.0/1.5$ (assumed)
Three fitting parameters in the mass exchange term: γ_1/γ_2	$2.96/3.13$ (fitted from the Richards model)

assuming the values, we have chosen the following approach to determine γ_1 and γ_2 . We solved the steady-state Richards equation for water transport in the MPL and GDL under simple boundary conditions: a constant water input flux at the bottom of MPL and zero saturation at the top of GDL. The same interface conditions as in Eqs. (8) and (9), and geometric and physical parameters as listed in Table 1 were used. No land area was included. Therefore, we had a 1D flow situation. Under these conditions, the water mass flux between the two layers, $S_w^T|_1$ or $S_w^B|_2$, was simply equal to the imposed input flux. From equations (13) and (14), with all parameters known, the value of the function f could be determined. These simulations were repeated for a wide range of input flux values and the results were used to prepare a plot of f versus input flux. The results are shown in Fig. 3, where also the average saturations s_1^w and s_2^w in the MPL and GDL respectively, are plotted. Then, Eq. (16) was fitted to the results and values of γ_1 and γ_2 were determined. We obtained the following numerically-fitted f function:

$$f(s_1^w, s_2^w) = \frac{(s_1^w)^{2.96} + (s_2^w)^{3.13}}{2.0} \quad (25)$$

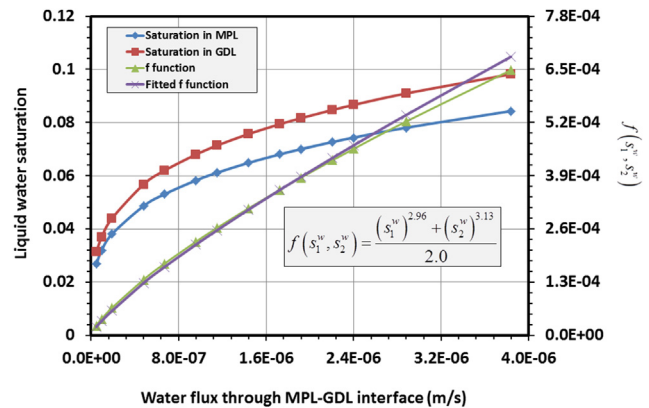


Fig. 3 – Numerical fitting of $f(s_1^w, s_2^w)$ as a function of the two saturations in the GDL and MPL.

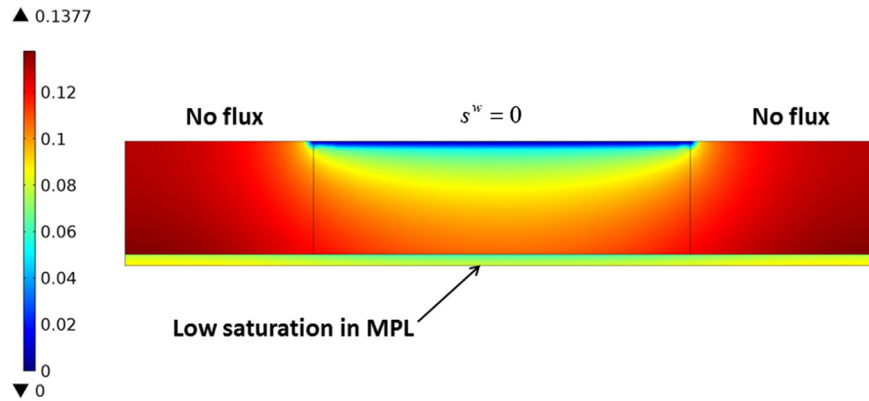


Fig. 4 – Water saturation distributions in the GDL and MPL from the 2D Richards model.

It is interesting to note that the values of γ_1 and γ_2 are quite close to 3, which is the exponent of saturation for the water relative permeability used in the Richards model. In the present work, Eq. (25) was used in all simulations involving the reduced continua model. Finally, it is worth noting that, strictly speaking, the Richards equation cannot be used in the through-plane direction of a discretized GDL, because the identification of an appropriate REV is not possible.

In what follows, we first compare results obtained from the two models, to show the potentials of the proposed reduced continua approach for modeling thin porous layers. Then, we discuss results of sensitivity studies using the reduced continua model.

Results and discussion

Comparisons between 2D Richards and 1D reduced continua models

First, we show the steady-state saturation distribution in the MPL and GDL obtained from the Richards model. As seen in Fig. 4, at steady state, significantly lower saturations are found in the MPL than in the GDL; this is explained by the fact that the MPL has a much finer pore structure than the GDL, and they are both hydrophobic. In the GDL, relatively low saturation is found under the channel area, and high saturation under the land areas. This is due to the fact that water under the land areas has to travel a longer pathway to exit to the GC [9].

Next, we compare steady-state water distributions along the in-plane direction (i.e. x direction) obtained from the Richards model and reduced continua model. For these simulations, the value of geometric constant, d (see Eq. (22)), was set equal to either 2.0 or 1.5. Note that, for the sake of comparison, water saturation obtained from the 2D Richards model is averaged over the layer thickness. As shown in Fig. 5, compared to the Richards model, the reduced continua model predicts lower water saturation in the GDL, particularly under the channel area. In the MPL, it predicts a little lower saturation under the land areas. Note that changing the value of the parameter d has a small effect on the results of the reduced

continua model for the GDL, but no effect on the results for the MPL. In the base case, the overall water contents in the GDL and MPL predicted by the reduced continua model are around 14% and 1.3% less than those from the Richards model, respectively.

In comparison to the Richards modeling, it is seen that the geometrically thin MPL can be well simulated by the reduced continua model. But, less water flooding in the GDL, particularly under the channel area, is predicted by the reduced continua model. This is mainly because the reduced continua model averages out macroscale saturation gradient along the layer thickness due to the failure of the REV concept. In laboratorial experiments, in-plane water distribution in GDL was visualized by means of synchrotron X-ray radiography [33,34]. It was found that much less liquid water accumulated under the channel area than under the land areas. This may be seen as a qualitative validation of the proposed reduced continua model. However, it is noted that, GDL can become compressed under the land areas [35] (this is not considered in the present

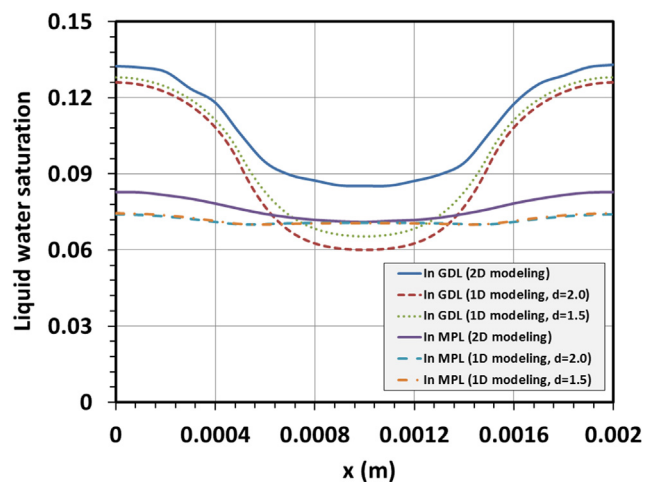


Fig. 5 – Steady-state water saturation distributions along the in-plane direction obtained from the 2D Richards modeling and 1D reduced continua modeling. For the sake of comparison, water saturation obtained from the 2D Richards model is averaged over the layer thickness.

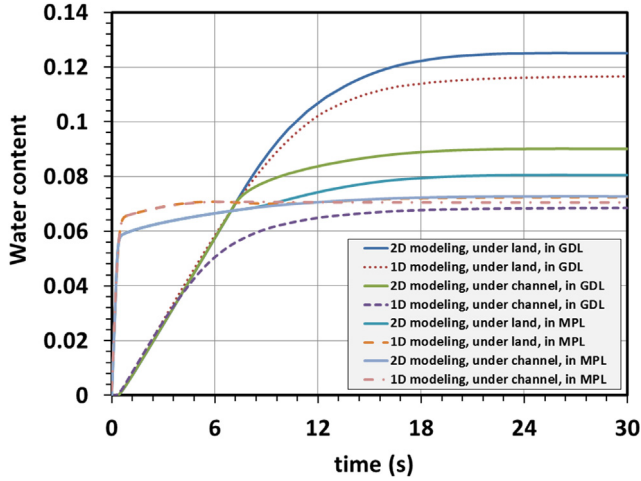


Fig. 6 – Temporal evolution of water contents averaged over the channel area and two land areas in the GDL and MPL obtained from the Richards model and reduced continua model.

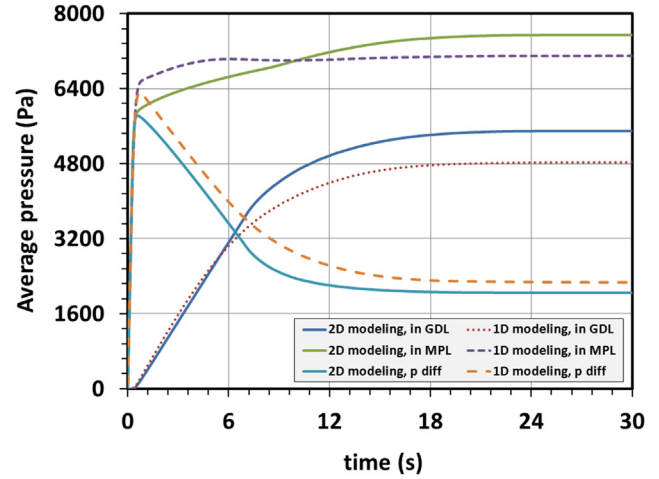


Fig. 7 – Temporal evolution of average water pressures in the GDL and MPL, as well as the pressure difference between the two domains.

work), which may also result in high water saturation due to the reduced permeability to water flow.

Finally, results of transient simulations with the two models are presented. Fig. 6 shows the temporal evolution of water contents averaged over the channel area and land areas in the GDL and MPL obtained from the two models. Fig. 7 shows the temporal evolution of average water pressure in each layer and the pressure difference between the two layers. Here again, the two models predict quite similar water dynamics in the MPL. But, the reduced continua model predicts much lower water content under the channel area in the GDL. The water content in the MPL increases fast at the beginning, then slowly reaches its steady-state value. As seen in Fig. 7, at the beginning, in a short time high water pressure builds up in the MPL. This is because the MPL is very thin and has a lower permeability. In the GDL, water pressure has a linear increase to its steady-state value.

Sensitivity studies using the reduced continua model

A major component of the reduced continua model is the constitutive equation (13) for mass exchange between two adjacent layers. In this paper, the material coefficient Π_m is parameterized by Eq. (14). This equation assumes that there is a perfect contact between the two layers. But, it is known that the presence of a physical interface between the two layers affects the mass exchange between them. In PEFC applications, cracks and gaps at the CL-MPL interface have a detrimental impact on the cell performance [14]. Kalidindi et al. [13] showed that the CL-MPL interface retained liquid water and induced mass transport resistance, resulting in nearly a 20% reduction in the limiting current density. We propose to model the imperfect contact between the two layers by introducing a correction factor m . Thus, equation (14) is rewritten as:

$$\Pi_m = m \frac{2}{b_1 + b_2} \rho_w \bar{k}_0 f(s_1^w, s_2^w) \quad (26)$$

where $0 \leq m \leq 1$, with the value of unity representing a perfect contact between the layers. The value of this correction factor depends on the morphology of layer–layer contact surface, which needs to be determined by experiments as part of the material property Π_m . Here, we simply varied its value to investigate the effect of layer–layer contact surface on the water flooding in the porous layers. Notice that, in reality, the MPL is often coated on one side of the GDL. So, the MPL-GDL interface would be much less important than the CL-MPL interface. However, in this work, we assumed imperfect contact between the MPL and GDL, in order to demonstrate that the reduced continua model can handle this effect easily and physically. Its application to the CL-MPL interface is straightforward.

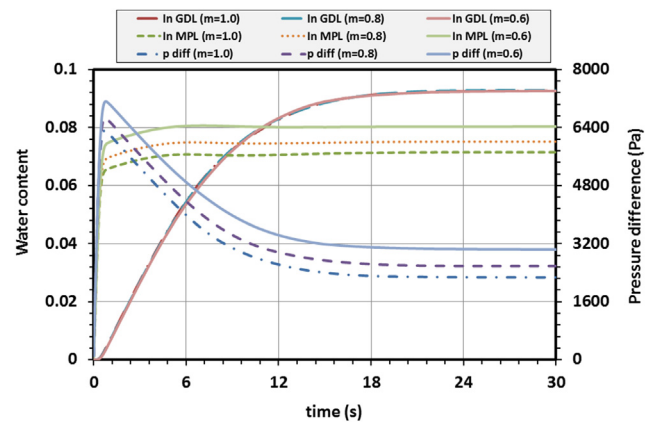


Fig. 8 – Effect of layer–layer contact parameter m on the water flooding the MPL and GDL, as well as the pressure difference between the two layers.

In Fig. 8, the temporal evolution of water contents and the pressure difference between the two layers are shown for values of $m = 0.6, 0.8$, and 1.0 . First, it is seen that the imperfect layer–layer contact has no significant effect on the temporal evolution of water content in the GDL. But, it has an important effect on the evolution of water content in the MPL. Poor layer–layer contact (i.e. small correction factor) would result in severe water flooding in the MPL. Also, as expected, the pressure difference between the two layers increases with the decrease in the correction factor. It is worth noting that the effect of imperfect contact between the two layers can be naturally included in the reduced continua model by experimentally determining the value of the material coefficient Π_m . However, it is not straightforward to include such effect in the Richards model.

According to the reduced continua model (cf. Eq. (15)), larger MPL thickness or GDL thickness would reduce the mass exchange between the two layers; consequently, more liquid water will accumulate inside the MPL. As shown in Fig. 9, at steady state, water saturation in the MPL increases almost linearly with increasing the MPL thickness. The same trend was found in the Richards model [30]. But, water saturation in the GDL is not affected by varying the MPL thickness. Fig. 10 shows the water content evolution with time in the MPL and GDL for five different MPL thicknesses. It is obvious that a thicker MPL has a larger water storage capacity. So, it is seen that increasing the MPL thickness would delay liquid water accumulation in the GDL; but, it does not influence the steady-state water content in the GDL. Fig. 11 shows the effect of GDL thickness on the steady-state water distributions. It is seen that water saturation in the MPL increases with the increase of the GDL thickness, particularly under the channel area. In the GDL, with the increase of its thickness, water saturation under the land areas decreases, but, water saturation under the channel area increases.

Finally, we investigated the influence of GDL anisotropy on the steady-state water distributions in the MPL and GDL. It is known that the commercially used carbon-paper or carbon-cloth GDL has a strong anisotropic nature with higher in-

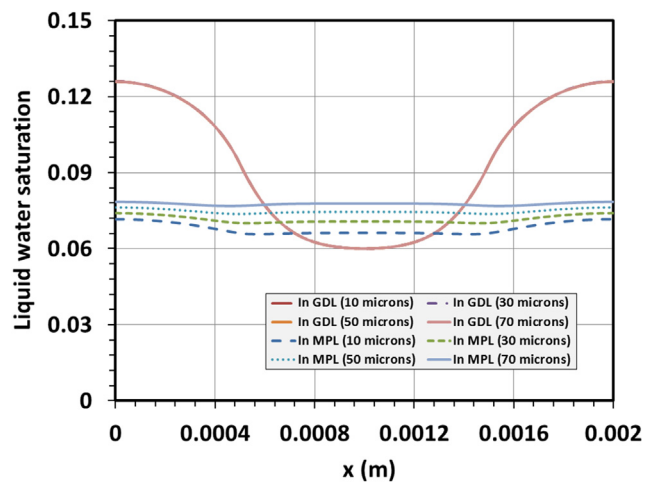


Fig. 9 – Effect of the MPL thickness (given in parenthesis) on the steady-state water distributions in the MPL and GDL.

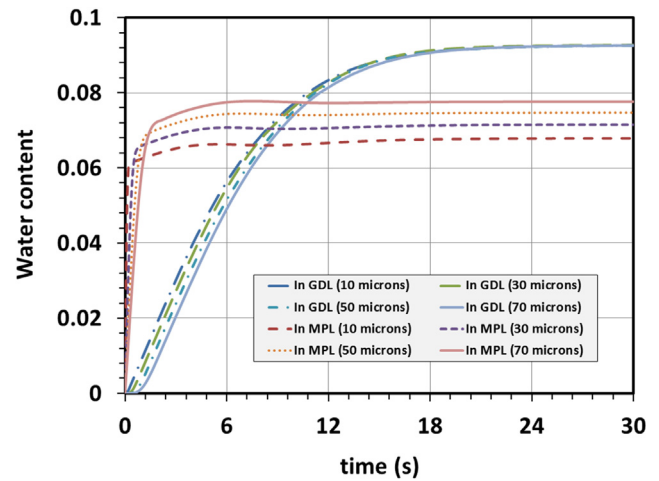


Fig. 10 – Effect of the MPL thickness on the temporal evolution of water contents in the MPL and GDL.

plane permeability. Results of simulation with a fixed water input and through-plane permeability, but larger in-plane permeability are shown in Fig. 12. The reduced continua model predicts that a GDL with high anisotropy can alleviate water flooding under the land areas dramatically, but the water saturation under the channel area is affected only slightly. This is because a GDL with higher in-plane permeability can transport accumulated water into the channel region more effectively. But, the water saturation in the fine MPL is not affected by varying the GDL anisotropy, as one would expect.

Conclusions and future work

The applicability of 3D Darcy-based models to the GDL is very questionable. This is mainly because the GDL thickness is only 10–15 times its pore size. To highlight this issue, in this work,

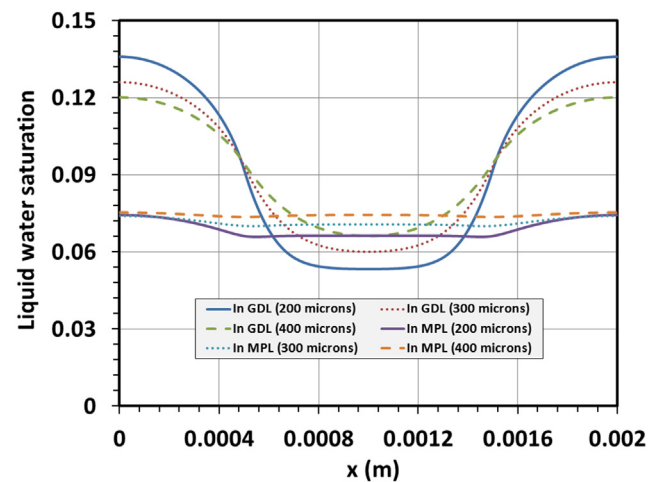


Fig. 11 – Effect of the GDL thickness (given in parenthesis) on the steady-state water distributions in the MPL and GDL.

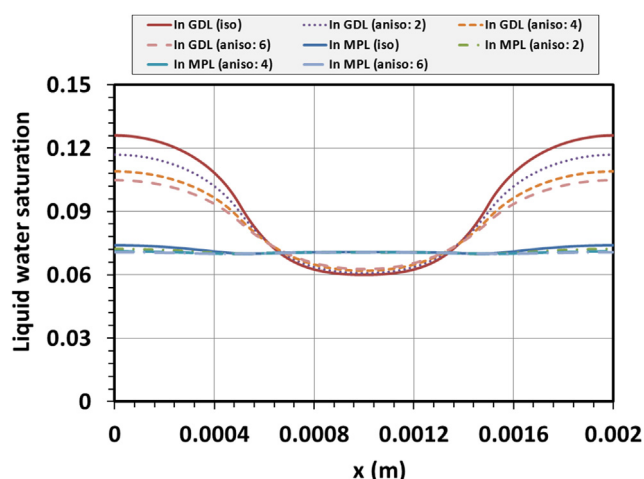


Fig. 12 – Effect of the GDL anisotropy on the steady-state water distributions in the MPL and GDL.

two types of numerical models were used to simulate liquid water dynamics in the MPL and GDL of a PEFC. One model is a traditional Darcy-based model (i.e. the Richards model); the other is the recently proposed thermodynamics-based reduced continua model. By comparing the numerical results obtained from the two models for identical boundary conditions, we reached the following main conclusions:

1. To capture similar dynamic behaviors of liquid water in the MPL and GDL, the reduced continua model requires enormously less computational efforts; only 150 edge elements compared to 25025 triangular elements required for the Richards model.
2. Compared to the Richards model, the thickness-averaged reduced continua model predicts less water flooding in the GDL, particularly under the channel area. This is because the reduced continua model averages out the macroscale saturation gradient along the layer thickness. This may suggest that the reduced continua model result is closer to the reality due to the failure of the REV concept in the GDL; a claim that needs to be verified by experiments.
3. The contact condition of the interface between the two layers has no influence on the dynamics of water flooding in the GDL, but has a considerable effect on the water evolution in the MPL. A poor layer–layer contact (i.e. small mass exchange capacity) results in severe water flooding in the MPL. The imperfect contact between neighboring layers can be easily implemented into the reduced continua model by experimentally determining the material property Π_m . Such a feature cannot be naturally included in the Richards model.
4. Sensitivity studies show that the reduced continua model can provide a fast evaluation of effects of material properties, such as layer thickness and permeability, on water flooding in the GDL and MPL.

A weakness of the reduced continua model would be that in the GDL, through-plane distribution of quantities plays a very important role in the overall transport phenomena. For

instance, temperature distribution would determine the water condensation and evaporation, and we may have local condensation controlled by local temperature. In cases that detailed small scale distribution of a quantity is needed, one can employ pore-scale modeling to simulate the through-plane distribution of that quantity. This can be then coupled to the reduced continua model of the whole fuel cell or stacks.

The proposed reduced continua model is still at its early stage. It needs to be improved, in the near future, by addressing the following issues:

1. The postulated form of material coefficient Π_m appearing in the mass exchange term (see Eq. (14)) needs to be validated and improved by experiments, in particular, regarding its dependence on the water saturations of neighboring layers.
2. In order to implement electrochemical reactions in CL as well as phase change between water vapor and liquid water, the rates of species mass exchange and heat exchange between neighboring layers need to be parameterized.
3. Combining the reduced continua model with pore-scale modeling of GDL would give the possibility of multi-scale modeling of a PEFC unit.

Acknowledgments

The authors are members of the International Research Training Group NUPUS, financed by the German Research Foundation (DFG) and The Netherlands Organization for Scientific Research (NWO).

REFERENCES

- [1] Weber Z, Newman J. Modeling transport in polymer-electrolyte fuel cells. *Chem Rev* 2004;104:4679–726.
- [2] Djilali N. Computational modelling of polymer electrolyte membrane (PEM) fuel cells: challenges and opportunities. *Energy* 2007;32:269–80.
- [3] Mench MM. Fuel cell engines. John Wiley & Sons; 2008.
- [4] Wang CY. Fundamental models for fuel cell engineering. *Chem Rev* 2004;104:4727–65.
- [5] Hoogers G. Fuel cell technology handbook. CRC Press; 2003.
- [6] Zhang S, Yuan XZ, Hin JNC, Wang H, Friedrich KA, Schulze M. A review of platinum-based catalyst layer degradation in proton exchange membrane fuel cells. *J Power Sources* 2009;194:588–600.
- [7] Mukundan R, Borup RL. Visualising liquid water in PEM fuel cells using neutron imaging. *Fuel Cells* 2009;09:499–505.
- [8] Li H, Tang Y, Wang Z, Shi Z, Wu S, Song D, et al. A review of water flooding issues in the proton exchange membrane fuel cell. *J Power Sources* 2008;178:103–17.
- [9] Qin CZ, Rensink D, Fell S, Hassanizadeh SM. Two-phase flow modeling for the cathode side of a polymer electrolyte fuel cell. *J Power Sources* 2012;197:136–44.
- [10] Ye Q, Nguyen TV. Three-dimensional simulation of liquid water distribution in a PEMFC with experimentally measured capillary functions. *J Electrochem Soc* 2007;154:B1242–51.

- [11] Hussaini IS, Wang CY. Visualization and quantification of cathode channel flooding in PEM fuel cells. *J Power Sources* 2009;187:444–51.
- [12] Wargo EA, Schulz VP, Cecen A, Kalidindi SR, Kumbur EC. Resolving macro-and micro-porous layer interaction in polymer electrolyte fuel cells using focused ion beam and X-ray computed tomography. *Electrochim Acta* 2013;87:201–12.
- [13] Kalidindi AR, Taspinar R, Litster S, Kumbur EC. A two-phase model for studying the role of microporous layer and catalyst layer interface on polymer electrolyte fuel cell performance. *Int J Hydrogen Energy* 2013;38:9297–309.
- [14] Swamy T, Kumbur EC, Mench MM. Characterization of interfacial structure in PEFCs: water storage and contact resistance model. *J Electrochem Soc* 2010;157:B77–85.
- [15] Basu S, Wang CY, Chen KS. Phase change in a polymer electrolyte fuel cell. *J Electrochem Soc* 2009;156:B748–56.
- [16] Wang Y. Modeling of two-phase transport in the diffusion media of polymer electrolyte fuel cells. *J Power Sources* 2008;185:261–71.
- [17] Berning T, Odgaard M, Kær SK. A computational analysis of multiphase flow through PEMFC cathode porous media using the multifluid approach. *J Electrochem Soc* 2009;156:B1301–11.
- [18] Bear J. Dynamics of fluids in porous media. American Elsevier; 1972.
- [19] Rebai M, Prat M. Scale effect and two-phase flow in a thin hydrophobic porous layer: application to water transport in gas diffusion layers of proton exchange membrane fuel cells. *J Power Sources* 2009;2:534–43.
- [20] Gostick JT, Fowler MW, Pritzker MD, Ioannidis MA, Behra LM. In-plane and through-plane gas permeability of carbon fiber electrode backing layers. *J Power Sources* 2006;162:228–38.
- [21] Gostick JT, Ioannidis MA, Fowler MV, Pritzker MD. Direct measurement of the capillary pressure characteristics of water–air–gas diffusion layer systems for PEM fuel cells. *Electrochem Commun* 2008;10:1520–3.
- [22] Hussaini IS, Wang CY. Measurement of relative permeability of fuel cell diffusion media. *J Power Sources* 2010;195:3830–40.
- [23] Rosén T, Eller J, Kang J, Prasianakis NI, Mantzaras J, Büchi FN. Saturation dependent effective transport properties of PEFC gas diffusion layers. *J Electrochem Soc* 2012;159:F536–44.
- [24] Qin CZ, Hassanizadeh SM. Multiphase flow through multilayers of thin porous media: general balance equations and constitutive relationships for a solid–gas–liquid three-phase system. *Int J Heat Mass Transf* 2014;70:693–708.
- [25] Meng H, Wang CY. Model of two-phase flow and flooding dynamics in polymer electrolyte fuel cells. *J Electrochem Soc* 2005;152:A1733–41.
- [26] Ju H. Investigation of the effects of the anisotropy of gas-diffusion layers on heat and water transport in polymer electrolyte fuel cells. *J Power Sources* 2009;191:259–68.
- [27] Wang Y, Basu S, Wang CY. Modeling two-phase flow in PEM fuel cell channels. *J Power Sources* 2008;179:603–17.
- [28] Wang XH, Nguyen TV. Modeling the effects of capillary property of porous media on the performance of the cathode of a PEMFC. *J Electrochem Soc* 2008;155:B1058–92.
- [29] Natarajan D, Nguyen TV. A two-dimensional, two-phase, multicomponent, transient model for the cathode of a proton exchange membrane fuel cell using conventional gas distributors. *J Electrochem Soc* 2001;148:A1324–35.
- [30] Pasaogullari U, Wang CY. Two-phase transport and the role of micro-porous layer in polymer electrolyte fuel cells. *Electrochim Acta* 2004;49:4359–69.
- [31] Qin CZ, Hassanizadeh SM, Rensink D, Fell S. One-dimensional phenomenological model for liquid water flooding in cathode gas channel of a polymer electrolyte fuel cell. *J Electrochem Soc* 2012;159:B737–45.
- [32] Qin CZ, Hassanizadeh SM, Rensink D. Numerical studies on liquid water flooding in gas channels used in polymer electrolyte fuel cells. *Chem Eng Sci* 2012;82:223–31.
- [33] Hartnig C, Manke I, Kuhn R, Kleinau S, Goebbels J, Banhart J. High-resolution in-plane investigation of the water evolution and transport in PEM fuel cells. *J Power Sources* 2009;188:468–74.
- [34] Eller J, Roth J, Gaudenzi R, Irvine S, Marone F, Stampanoni M, et al. Water distribution in GDL near optimal humidification. *ECS Trans* 2012;50:477–86.
- [35] Nitta I, Hottinen T, Himanen O, Mikkola M. Inhomogeneous compression of PEMFC gas diffusion layer. Part 1. *Exp J Power Sources* 2007;171:26–36.

Glossary

- b: porous layer thickness (m)
d: fitting parameter in Eq. (22) (–)
 g_x : gravity component in the x direction (m s^{-2})
 g : gravity vector (m s^{-2})
I: cell operating current density (A m^{-2})
j: water flux (m s^{-1})
J: Leveret-J function (–)
 k : intrinsic permeability (m^2)
 k^r : relative permeability (–)
 k_i : in-plane permeability (m^2)
 k_t : through-plane permeability (m^2)
 k_t : intrinsic permeability of the two layers defined in Eq. (15) (m^2)
 $M_{\text{H}_2\text{O}}$: molecular weight of water (kg mol^{-1})
p: pressure (Pa)
s: liquid water saturation (–)
S: mass source/sink term in the interacting continua model ($\text{kg m}^{-2} \text{s}^{-1}$)
t: time (s)
T: stress input in Eq. (17) and Eq. (18) ($\text{m}^2 \text{s}^{-2}$)
v: 1D velocity (m s^{-1})
 \mathbf{v} : 2D velocity vector (m s^{-1})
 Π_m : material property in Eq. (13) (s m^{-1})
 Ω : wettability potential in Eq. (17) (Pa)

Greek letters

- ρ : mass density (kg m^{-3})
 ϵ : porosity (–)
 μ : dynamics viscosity (Pa s)
 σ : air–water surface tension (N m^{-1})
 θ : contact angle of porous layer ($^\circ$)
 γ_1, γ_2 : two fitting parameters in the mass exchange term in Eq. (21) (–)

Superscripts

- w: liquid water
a: air phase
c: Capillary
0: Intrinsic
r: Relative
B,T: bottom, top

Subscripts

- MPL: micro porous layer
GDL: gas diffusion layer
1,2: first layer (MPL), second layer (GDL)
w: liquid water